21st Australasian Fluid Mechanics Conference
Adelaide, Australia
10-13 December 2018

Temporal Numerical Simulation of Atomization of Liquid Jet using Diffuse Interface Model

H. Sugiura[1], K. Tsujimoto[1], T. Shakouchi[1] and T. Ando[1]

[1]Division of Mechanical Engineering, Graduate School of Engineering
Mie University, Kurimamachiya-cho 1577, Tsu, Mie, 514-8507 Japan

Abstract

An improvement of atomization of liquid jets requires in several engineering applications. Although a large number of studies have been performed on the breakup process of liquid jets so far, the mechanisms of breakup contributing to the performance of atomization have not well revealed yet. Hence, in the present paper as a predictably effective method to analyze the breakup process, a temporal numerical simulation is proposed. As the remarkable features of the numerical scheme, a Cahn-Hilliard equation is employed to track the interface of gas-liquid two-phase flow. In order to examine the possibilities of the proposed method, we conduct the three-dimensional simulation of the temporal developing liquid jet. Further, we investigate the effects of a duplex nozzle represented by convex or concave inflow velocity profile on the development of liquid jet and demonstrate the usefulness of the duplex nozzle for atomization.

Introduction

Liquid atomization technology is applied to fuel spray in an engine, spray printing, spray drying and powder producing. The advancement of these technologies needs flow control based on the elucidation of a detailed mechanism of the atomization. Until now, although a large amount of knowledge about atomization has shown, the detailed mechanism to the final atomization state is not enough to make clear. In general, although numerical analysis is an effective method in the elucidation of the mechanism of the atomization, to reproduce fine scale droplets, high grid resolution is inevitably required. Recently, it has succeeded a large-scale computation of spatially developing liquid jet and demonstrated the detailed process to droplet generation[10]. Also, to improve the atomization of a liquid jet, various types of inflow velocity distribution mimicked short or long nozzle, diverging nozzle, duplex nozzle, etc. numerically are examined in 2D simulations of spatially-developing plane liquid jets by Sander et al.[11]. Among of these nozzles, they found that the duplex nozzle causes the most efficient jet spreading, however, because of low *We* number, breakup of liquid jet, i.e., atomization is not well predicted[11]. In our previous study[12], in order to investigate whether small-scale computation is capable of capturing details of liquid jet, we conducted a temporal simulation of plane liquid jet by DIM (diffuse interface model)[1, 6] based on the Cahn- Hilliard equation[4], and demonstrated clearly that the temporal simulation is capable of correctly reproducing behavior of the breakup process.
In this study, we pay attention to the performance of duplex nozzle in relative high *We* number as considering actual liquid jet, and investigate the effects of two inflow conditions (concave or convex) on the breakup process of plane liquid jets using our proposed temporal simulation.

Numerical method

Governing equations and their discretization

Assuming incompressible flow for each phase, the governing equations are as follows:

$$\nabla \cdot \boldsymbol{u} = 0 \tag{1}$$

$$\frac{D\boldsymbol{u}}{Dt} = -\frac{1}{\rho}\nabla p + \nabla \cdot \boldsymbol{\tau} + \frac{1}{\rho}\boldsymbol{f}_s \tag{2}$$

$$\frac{D\phi}{Dt} = \frac{1}{\mathrm{Pe}}\nabla^2 \mu_c \tag{3}$$

$$\boldsymbol{f}_s = -\sigma\kappa\nabla\phi \tag{4}$$

where $\boldsymbol{u}$ is the velocity, p, ρ, and μ are the pressure, the density, and the viscosity, respectively. σ denotes the coefficient of surface tension. ϕ, Pe, and μ_c denote an order parameter, the Peclet number, and chemical potential, respectively. The physical quantities are defined with those of each phase, i.e., where subscript g and l denote gas and liquid phase, respectively.

$$\rho = \frac{1}{2}\left[\rho_l(\phi+1) - \rho_g(\phi-1)\right] \tag{5}$$

$$\mu = \frac{1}{2}\left[\mu_l(\phi+1) - \mu_g(\phi-1)\right] \tag{6}$$

The third term of r.h.s. of equation (2) is the surface tension force. In general, for the DIM the surface tension force is derived based on the energy minimization[6], and conventional form of surface tension is constructed with the chemical potential and the gradient of the order parameter[6]. On the other hand, CSF (continuous surface tension) model proposed by Brackbill[3] is widely used in multiphase flow computations. Instead of the conventional form. Kim introduces the CSF model into the DIM and demonstrates the usefulness of CSF model[7]. In our experience, we also find that when the interface thickness of DIM is thin the CSF model is superior to the conventional form to track the interface profile. Thus in the present simulation, we adopt the CSF model.
So as to capture fine scale droplet as far as possible, the spatial discretization is conducted with a fourth-order finite difference scheme on a staggered grid. Because of the large-density ratio between two phases, it is difficult to an iteratively solve the pressure Poisson equation. In the present simulation, BiCGSTAB method [13] is adopted as iterative method. It is well known that the introduction of an upwinding scheme for the convective terms is useful to suppress the numerical instability. In the present simulation, QUICK method is employed to discretize the convective terms. Further, in order to suppress the spurious current, we introduce (i) balanced-force algorithm for the reduction of discretized error due to the discrepancy between a pressure gradient and surface tension force[5], (ii) accurate interpolation for the curvature estimation[14], and (iii) accurate estimation of curvature using filtered order parameter $\tilde{\phi}$ as follows:

$$\kappa = \nabla \cdot \left(\frac{\nabla\tilde{\phi}}{|\nabla\tilde{\phi}|} \right) \tag{7}$$

Cahn-Hilliard equation

In the DIM[1], interface profiles are constructed as follows: the interface between different phases is assumed to have finite

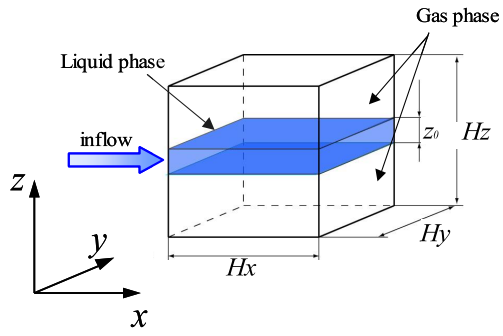

Figure 1: Flow domain and coordinate system

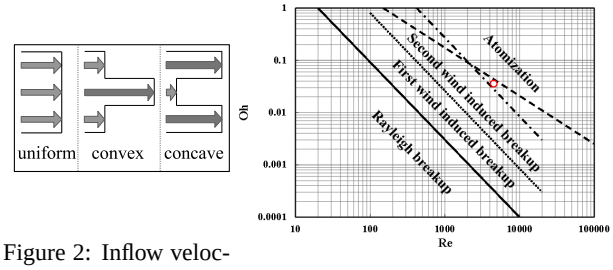

Figure 2: Inflow velocity profiles

Figure 3: Ohnesorge chart for liquid jet

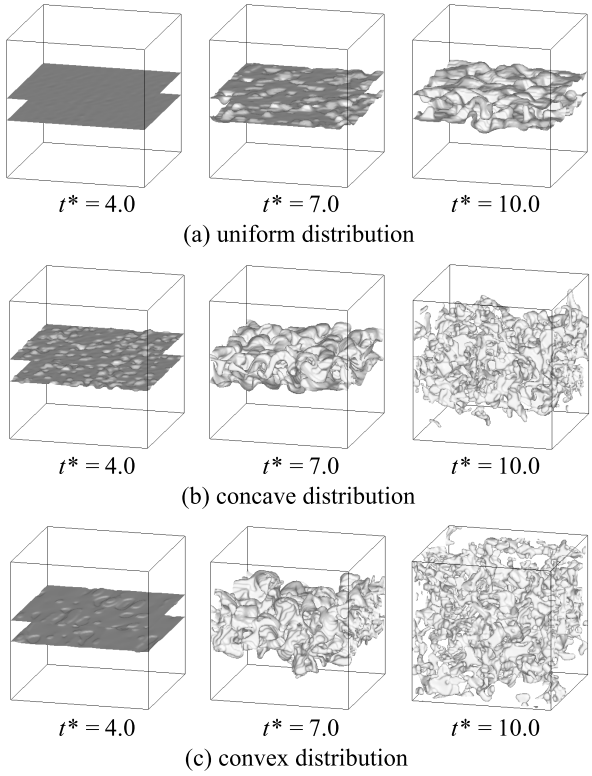

Figure 4: Visualization of liquid jet at $t^* = 4.0, 7.0, 10.0$

thickness; the physical quantities are continuously distributed inside the finite thickness of interface; the profiles of interface are determined based on the free energy of a considering system.

The order parameter ϕ corresponding to the mass density of, or the concentration of fluids is introduced, then the free energy, $F(\phi)$ can be described as a function of ϕ:

$$F[\phi] = \int_V \left\{ f(\phi(x)) + \frac{1}{2}\kappa|\nabla\phi(x)|^2 \right\} dV \tag{8}$$

$$\mu_c(\phi) = \frac{\delta F[\phi]}{\delta\phi(x)} = f'(\phi) - \xi^2\nabla^2\phi \tag{9}$$

where $f'(\phi)$ is $f'(\phi) = \phi^3 - \phi$. ξ corresponds to the interface thickness. The chemical potential μ_c can be found by minimizing the free energy, F. The interface diffusion fluxes are assumed to be proportional to the gradient of the chemical potential, finally, as a convective Cahn-Hilliard equation, equation (3) is derived.

Calculation conditions

The flow considered in this study consists of a temporal evolving planar jet in a quiescent air. Figure 1 shows a coordinate system and a calculation domain. In the coordinate system, x is streamwise direction, y is spanwise direction and z is a liquid jet width direction. The periodic condition is applied for all direction as the boundary condition. The calculation domain is $H_x \times H_y \times H_z = 6z_0 \times 6z_0 \times 6z_0$ where z_0 is liquid jet width. The grid number is $n_x \times n_y \times n_z = 64 \times 120 \times 128$. The gravity term of the equation of motion is ignored. Reynolds number is $\mathrm{Re} = u_0 z_0/\nu_l = 4500$. Various types of inflow velocity distribution numerically are examined in the 2D spatially-developing plane liquid jet by Sander et al.[11]. They found that the duplex nozzle mimicked using convex or concave inflow velocity profile shown in figure 2, demonstrates the most efficient jet spreading, however, because of low *We* number (*We*=340), the breakup of the liquid jet, i.e., atomization is not well predicted[11].

In general, various breakup regimes are classified in the Ohensorge chart shown in figure 3. In the chart, the breakup regime is governed by *Oh* number ($Oh = \sqrt{We}/Re$) and Reynolds number[9]. In this study, in order to investigate further how the duplex nozzle effects to the breakup of the liquid jet, we have set 3 types of inflow distribution pattern shown in figure 2: Uniform inflow distribution with the maximum center velocity of the liquid jet as $u_c = u_0$; convex inflow distribution with $u_c = 2u_0$ and concave inflow distribution with $u_c = 1/4u_0$. In all cases, it is assumed that the flow rate is the same as uniform inflow. The Weber number of present simulation, $\mathrm{We} = \rho_l u_0^2 z_0/\sigma = 26036$ and the *Oh* number of present simulation is plotted with a red-color circle in the chart, corresponding to second wind-induced breakup in the vicinity of atomization.

Results

Time-evolving instantaneous flow fields

We demonstrate time-evolving instantaneous flow fields based on interfaces between gas an liquid and vortical structures.

Figures 4 show the images of the interface of uniform ($u_c = u_0$), convex ($u_c = 2u_0$) and concave ($u_c = 1/4u_0$) inflow velocity distribution at $t^* = 4, 7$ and 10 visualized with isocontour surface of order parameter $\phi(= 0)$. Regardless of inflow distribution, the interface wrinkles as time passes. In the uniform inflow distribution, the jet develops monotonically. On the other hand, in the convex and concave inflow distribution, the jet develops rapidly. At $t^* = 4.0$ and later, concave and convex inflow distributions are more rapidly disturbed than the uniform one, in particular, convex inflow distribution starts to break up at $t^* = 7.0$. In our previous work[12], although a treatment of conversion between temporal and spatial axis is rough, we found that it is capable of comparing with the results of temporal and spatial evolution using a relation of $t^* \approx x/z_0$. In

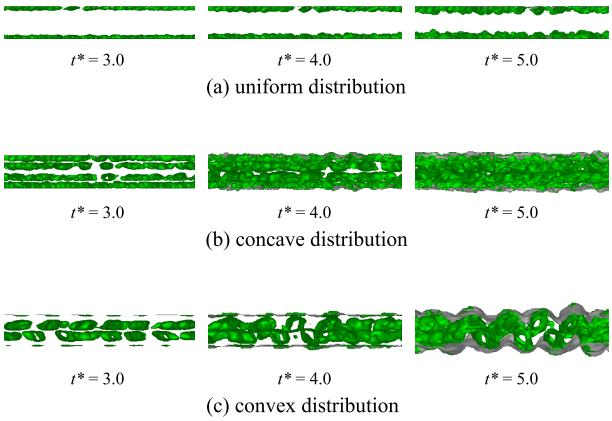

Figure 5: Visualization of vortex structure at $t^* = 4.0$, 7.0, 10.0

the results of Sander et al.[11] a uniform distribution demonstrates the only occurrence of wrinkles even at the downstream location, $x/z_0 = 16$, while in case of both concave and convex distribution, large transverse deformations of liquid jet begin to occur around $x/z_0 \approx 6$ or 7. Thus, it can be confirmed qualitatively that the present temporal evolving jet behaves similarly to the spatially-developing jet.

In order to elucidate the reason for jet spreading, vortical structures at $t^* = 3.0 \sim 5.0$ are visualized using the second invariant of the velocity gradient tensor, Q shown in figure 5.

At the initial stage, $t^* = 3.0$, for the uniform case, vortices are formed in the vicinity of the interface between liquid and gas; for the convex case, vortical structures which are generated at a place where internal shear corresponding to the convex velocity profile, coalesce and form larger-scale structures, inducing large deformation of liquid jet; for the concave case, the above-mentioned place which related to the interface and the internal shear contribute to the vortex generation. In addition, it can be confirmed that the generated vortical structures seem to be large scale roll structures, which is usually observed in developing mixing layers[2]. On the other hand, a different feature concerning growth rate is observed: the vortices generated due to internal shear promptly grow into the roll structures, but vortical structures in the vicinity of the interface slowly develop.

Mean flow properties

We demonstrate quantitatively the effect of the duplex nozzle on mean flow properties.

Figures 6 show the temporal variation of mean streamwise inflow velocity distribution. In uniform inflow distribution, the velocity gradient near the initial interface weakens as the time proceeds. These results are compared with spatially evolving liquid jet[8] and have been confirmed to be reasonable[12]. In convex inflow distribution, at the initial time ($t^* < 5.0$), the liquid jet scarcely expands but at the end, it rapidly expands and breaks up. Same behavior of the liquid jet can be seen at the visualized image (figure 4). In concave inflow distribution, it does not develop rapidly like convex inflow distribution, but after ($t^* = 7.5$), the behavior is similar.

Figures 7 show the fluctuation of streamwise velocity. In uniform inflow distribution, as the average speed in the mainstream direction develops, the fluctuation grows slowly at the location of shear. In both convex and concave inflow distribution, the fluctuation occurs depending on the initial inflow distribution up to $t^* < 5.0$, but after that, the flattened profile of fluctuation is governed by the large-scale roll structure mentioned before.

Figures 8 show the volume concentration of liquid which means the spread of the liquid jet. In uniform inflow distribution, the

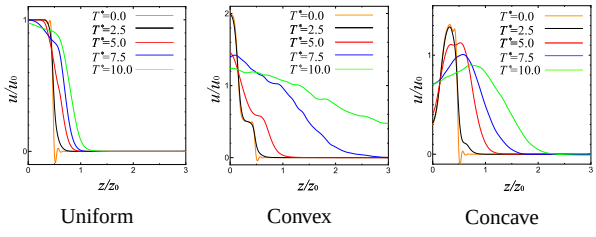

Figure 6: Mean axial velocity

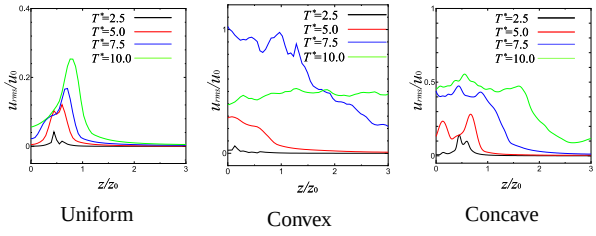

Figure 7: Mean axial velocity fluctuation

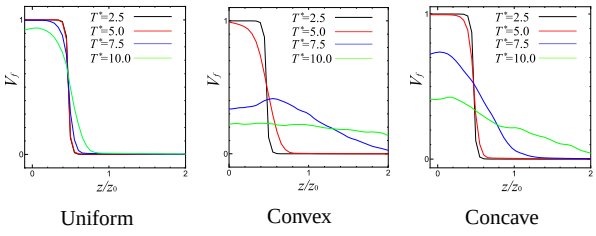

Figure 8: Mean volume concentration

volume concentration distribution changes gradually around the initial interface position of $z/z_0 = 0.5$. In both convex and concave inflow distribution, it diffuses to the surroundings as the flow expands and spreads. Especially at the end of the time, it spreads evenly.

Breakup characteristics

In order to calculate a number of droplet and droplet diameter, we explain the grouping procedure of cell including liquid. Figures 9 show the schematics of phase distribution on one $x-z$ plane. In the figure, blue and white color means gas and liquid (droplet), respectively, and the red color number is allocated for each cell. The cell belonging droplet should be grouped so that it is recognized as a part of one droplet. The grouping procedure of cell are as follows: (i) a droplet cell is sequentially allocated a number along with x direction. When a cell locates next to a droplet cell, the same number is allocated to a cell (figure 9(i)); (ii) the cell number is re-allocated along with decreasing x and z directions. If the lower number exists at the right- or lower side of the cell, the cell number is changed the lower one. As an example, The number “twelve’’ in figure 9(i) is changed to the number “ eleven’’ in figure 9(ii), while the number “seven’’ in figure 9(i) is remained because of the no existence of vapor cell around lower side; (iii) further, the cell number is re-allocated along with increasing x and z directions. If the lower number exists at the right or upper side of the cell, the cell number is changed the lower one (figure 9(iii)) ; (iv) after the step (ii)-(iii) is repeated a few times, the numbering is completely finished as shown figure 9(iv).

Figures 10 show a graph indicating the droplet diameter (equivalent sphere diameter) versus the number of droplets for each velocity distribution at $t^* = 10.0$. In figures 10, the horizontal axis is the droplet diameter, and the vertical axis is the number

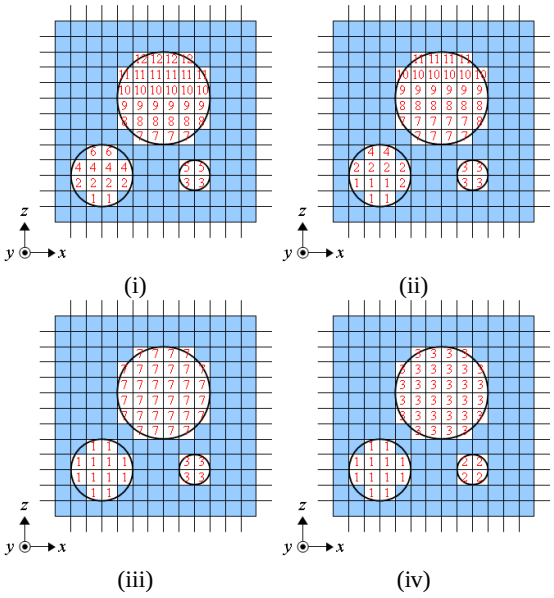

Figure 9: A numbering procedure of cell being located on the wall surface inside the droplet.

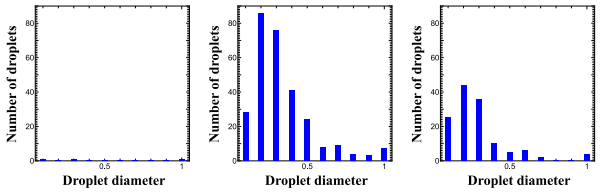

Figure 10: Evaluation of droplet diameter & number of droplets at $t^* = 10.0$

of generated droplets. For the uniform case (figure 10(a)) almost no liquid droplets are generated because of the liquid film does not break up within the present simulation time. While for the convex case, a large number of droplets are generated. About 81% of the particles having a diameter of 0.4 or less occupy among all the particles.

For the concave case, the same trend is shown in figure 10(b) i.e., the peak locates at the diameter of 0.2, and particles having a diameter of 0.4 or less is present in about 87% of all the particles.

From the above-mentioned results, it is confirmed that the atomization of the liquid jet is promoted with the convex and concave velocity distribution more than the uniform velocity distribution. In addition, comparing the convex and concave velocity distribution, the convex velocity distribution produces a lot of liquid droplets due to break up.

Conclusion

In this study, we carried out a time-evolved simulation of a planer liquid jet using a diffuse interface model and examined the effect of velocity distribution on the liquid jet behavior. The liquid jet becomes unstable and expands rapidly if the inflow velocity distribution is applied like a convex or concave than a uniform. When a convex and concave velocity distribution is applied, a roll vortex structures appear inside the jet and expands rapidly by this structure coalescence. From the comparison of the droplet diameter and the number of droplets, internal shear imposed on inlet contributes to generating droplets of small diameter at an early stage. In addition, the number of droplets is larger for the convex inflow distribution. Thus we confirm that concave or convex inflow corresponding to the duplex nozzle is useful for breakup of liquid jet even at the relative high *We* number.

References

[1] Badalassi, V.E., Ceniceros, H.D. and Banerjee, S., Computation of multiphase systems with phase field models, J. Comp. Physics, **190-2**, 2003, 371-397.

[2] Bernd, L.P. and Roshko, A., Streamwise vortex structure in plane mixing layers, J. Fluid Mech., **170**, 1986, 499-525.

[3] Brackbill, J.U., Lothe, D.B. and Zemach, C., A continuum method for modeling surface tension , J. Comp. Physics, **100**, 1992, 335-354.

[4] Cahn, J.W. and Hilliard, J.E., Free energy of a nonuniform system I. J. Chem. Phys., **28**, 1958, 258-267.

[5] Francois, M.M., Cummins, S.J., Dendy, E.D., Kothe, D.B., Sicilian, J.M. and Williams, M.W., A balanced force algorithm for continuous and sharp interfacial surface tension models within a volume tracking framework, J. Comp. Phys., **213**, 2006, 141-173.

[6] Jacqmin, D., Calculation of two-phase Navier-Stokes flows using phase-field modeling, J. Comp. Phys., **155**, 1999, 96-127.

[7] Kim, J., A continuous surface tension force formulation for diffuseinterface models, J. Comp. Phys., **204**, 2005, 784-804.

[8] Klein, M., Direct numerical simulation of a spatially developing water sheet at moderate Raynolds number, International Journal of Heat and Fluid Flow 26, 2005, 722-731.

[9] Reitz, R.D., Atomization and other breakup regimes of a liquid jet, Ph.D. thesis, Princeton University, Princeton, NJ, 1978.

[10] Shinjo, J. and Umemura, A., Simulation of liquid jet primary breakup : Dynamics of ligament and droplet formation, Int. J. Multiphase Flow, **36**, 2010, 513-532.

[11] Sander, W. and Weigand, B., Direct numerical simulation and analysis of instability enhancing parameters in liquid sheets at moderate Reynolds numbers., Phys. Fluids, **20**, 2008.

[12] Tsujimoto, K., Morishita, Y., Shakouchi, T. and Ando, T., Numerical Simulation of Liquid Jet using Diffuse Interface Model, Proc. Int. Conf. Multiphase Flow, 2013, 5P.

[13] Vorst, H.A., BiCGSTAB: A fast and smoothly converging variant of Bi-CG for the solution of non-symmetric linear systems, SIAMJ. Sci. Stat. Comput., **13**, 1992, 631-644.

[14] Yokoi, K., A practical numerical framework for free surface flows based on CLSVOF method, multimoment methods and densityscaled CSF model: Numerical simulations of droplet splashing, J. Comp. Phys., **232**, 2013, 252-271.